JOURNAL OF AIRCRAFT
Vol. 45, No. 3, May–June 2008

Improving Hang-Glider Maneuverability Using Multiple Winglets: A Numerical and Experimental Investigation

D. P. Coiro,* F. Nicolosi,† F. Scherillo,‡ and U. Maisto§
University of Naples "Federico II," 80125 Naples, Italy

DOI: 10.2514/1.33265

The main aim of this paper is to investigate the influence of multiple winglets on hang-glider climbing performance. The study aims to optimize the $C_L^{3/2}/C_D$ parameter. The investigation was performed both numerically and experimentally starting from airfoils and winglet shape design. Given the shape of a real hang-glider wing under aerodynamic load, the first phase of the work concerned the main geometric characteristics of winglet design: the number of winglets, airfoils, planform shape, and twist. A 3-D wing model was built and using the indications obtained from the design, different sets of winglets were built. The wing model was built to enable winglets to be applied to the wing tip without changing the wing span and aspect ratio. The tests carried out on the hang-glider model showed an improvement in wing performance of about 15%. However, the model reproduced a full-scale wing flying under aerodynamic load and, according to the model builders, it showed a positive twist angle (leading edge up). This could mean that the winglets were more efficient because the original wing showed a strong tip vortex. A new model wing with an elliptical planform was therefore built to verify this further. The test results on the elliptical wing did not show the same improvement in performance obtained with the hang-glider model. Nevertheless, compared to the original elliptical wing an improvement was still found.

Nomenclature

AR	=	aspect ratio
b	=	semispan
C_D	=	drag coefficient
C_{Di}	=	induced drag coefficient
C_L	=	lift coefficient
C_{L_α}	=	lift curve gradient
$C_L^{3/2}/C_D$	=	endurance coefficient
c	=	chord
cC_l	=	span load
c_r	=	root chord
c_t	=	tip chord
D_i	=	induced drag
e	=	Oswald factor
r	=	turn radius
S	=	semisurface
V_s	=	sinking rate
W	=	weight
α	=	angle of attack
ζ	=	vorticity
ρ	=	density
Φ	=	bank angle
ψ	=	streamline function

I. Introduction

EVER since man started to think about flying, he has striven to imitate the shape and structure of a bird wing. Large soaring birds such as the Peruvian condors (see Fig. 1) are able to soar at very high altitudes in very narrow thermals and this is probably in part due to their tip feathers called *remiges*. These are continuously moved and adapted to optimize flying under different flight conditions. Nowadays, composite materials, such as epoxy carbon fibers, allow very stiff structures to be built, even slender shapes such as remiges. The first investigations on a single winglet were performed by Whitcomb [1,2] in the mid-1970s and it was shown that, if properly designed, the winglet can improve efficiency by reducing the induced drag. Many other researchers have investigated their behavior, designing winglets for commercial and general aviation aircraft as well as for sailplanes [3].

Furthermore, the added friction and interference drag has to be canceled out by the forward thrust generated by the winglet lift. Because this has been proven to work, it is thus possible to extend this concept to multiple winglets. The principle is to spread the tip vortex in more vortices of less intensity. A variety of types of multiple winglets have been investigated by many authors in the past, such as Spillman et al. [4,5], Zimmer [6], La Roche and La Roche [7], and more recently by Smith et al. [8,9] and Catalano and Ceron-Munoz [10]. The importance of numerical accuracy and the difficulties in predicting the effect of winglets on drag using numerical methods have been well illustrated by Smith [11]. Different concepts, including box and ring wings, have been thoroughly analyzed by Kroo [12].

The main goal of this work is to investigate the influence of multiple winglets on the climbing performance of a hang glider. To this end, a set of winglets was designed and tested for application onto a hang-glider wing tip. As shown by Smith et al. [8,9] and Catalano and Ceron-Munoz [10], it appears that by using an opportunely designed set of remiges it is possible to improve wing performance by minimizing the hang-glider sink rate of Eq. (1). This is inversely proportional to the endurance parameter $C_L^{3/2}/C_D$. The main objective of this work is to improve this parameter:

$$V_s = \frac{1}{C_L^{3/2}/C_D} \cdot \frac{1}{\cos^{3/2}\Phi} \sqrt{\frac{2W}{\rho S}} = \frac{1}{C_L^{3/2}/C_D} \cdot \sqrt{\frac{2W}{\rho S}} \cdot \left[1 - \left(\frac{2W}{\rho S}\frac{1}{rgC_L}\right)^2\right]^{-\frac{3}{4}} \quad (1)$$

The winglets were designed for the wing of the hang glider belonging to Angelo D'Arrigo, a world champion hang-glider pilot and record

Presented as Paper 4435 at the 25th AIAA Applied Aerodynamics Conference, Miami, Florida, 25–28 June 2007; received 4 July 2007; revision received 18 November 2007; accepted for publication 19 November 2007.

*Professor, Department of Aerospace Engineering; coiro@unina.it.
†Assistant Professor, Department of Aerospace Engineering; fabrnico@unina.it.
‡Research Assistant, Department of Aerospace Engineering; scherill@unina.it.
§Engineer, Department of Aerospace Engineering; maistou@virgilio.it.

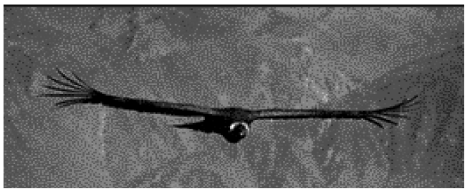

Fig. 1 Peruvian condor.

holder. He has flown his hang glider at 33,000 ft spiraling with condors. The ultimate aim of the optimization was to prove that it is possible to climb with a shorter wing (equipped with winglets) than the original, without losing any climbing performance but with gains in maneuverability. At very high altitudes, thermals are very narrow and in order to soar in them it is preferable to have a wing with a small span to maneuver in spirals, but this conflict with the high aspect ratio required one to climb with a minimum sink rate.

The winglets design process was performed using a classical vortex lattice method [13] to rapidly perform computations for many different configurations. The cant angle and twist of winglets were the main parameters to be optimized during the design phase. The design was carried out using two sets of remiges: one made of five and the other of three. The optimization was carried out by replacing part of the wing tip with the winglets to keep wing span the same and to preserve essentially the same aspect ratio of the "complete wing" so that the complete wing and the wing with winglets could be compared accurately.

Using the information obtained from the design phase, two sets of remiges of five and three winglets were built. A wing model on which to apply the winglets was also built. The wing model was designed and built so that a part of the wing tip could be extracted and replaced by the set of winglets. A further part of the wing could also be extracted and the remiges applied, thereby making it possible to test a shorter wing. The various configurations were tested in the wind tunnel of the Department of Aerospace Engineering of the University of Naples Federico II.

The actual wing model produced was characterized by a tip twist angle with positive (nose up) value. The builder did this to reproduce the real shape of a hang glider in flight. This tip twist angle led to an increase of the induced drag with respect to the same untwisted geometry, as can be easily shown through numerical analysis.

After the first series of experimental tests we decided to carry out new tests, building another wing model characterized by an elliptical shape to ensure an optimal span load distribution. The elliptical wing model was built along the same lines as the first, to allow a part of the wing tip to be replaced by the set of remiges.

II. Remiges Design

The underlying objective of the design process was to find the optimal configuration with respect to cant angle, length, and twist of the remiges in terms of the endurance parameter $C_L^{3/2}/C_D$. The investigation was carried out using a classical vortex lattice method. As stated above, a part of the hang-glider wing was substituted with a set of different remiges with different cant angles, pitch angles, and twist.

The main wing airfoil is shown in Fig. 2. The SD-7032[¶] airfoil was chosen for the remiges (Fig. 3).

Both configurations with two and three remiges were investigated.

The typical mesh contained 10 panels chordwise and 35 panels spanwise giving about 350 panels for the total wing and about 320 panels for the configuration with remiges (Fig. 4).

The span of the remiges was chosen by looking at the distribution of upwash velocities induced in the span direction and outside of the cut wing (shorter wing) adjusting the remiges length to obtain same span of the complete wing (see also [10]). A remige length of about 17% of the total wing span resulted from this investigation. During

[¶]Data available online at http://www.ae.uiuc.edu/m-selig/ads/coord_database.html [retrieved 20 May 2006].

Fig. 2 Main wing airfoil "Stratos" hang glider.

Fig. 3 Remiges airfoil: SD-7032.

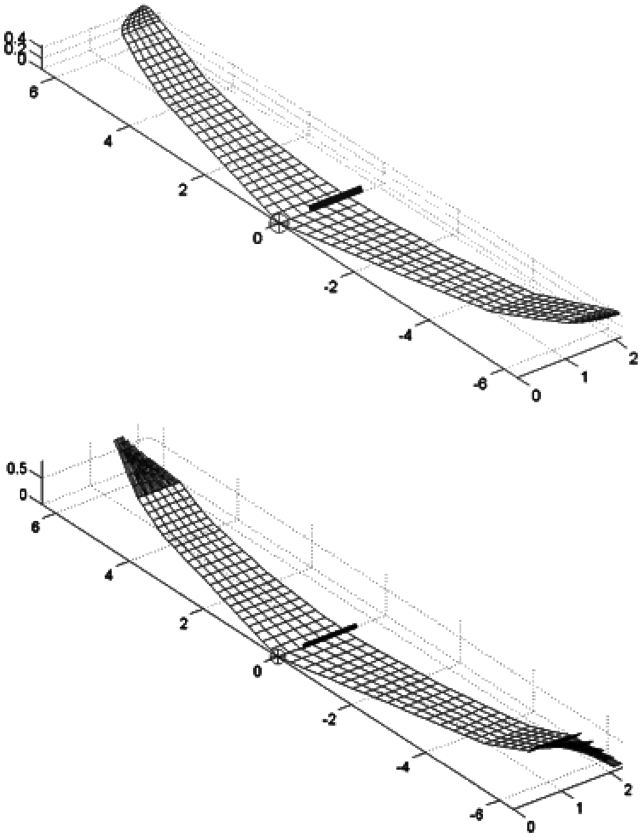

Fig. 4 Total and five-remiges wing: grid examples.

the numerical investigation many different combinations of cant and twist angles were tested and compared.

The numerical results suggested that it is better to increase the cant angle as much as possible, to maximize the distance between the remiges. The twist angles are reported in Tables 1 and 2. The twist

Table 1 Five-remiges twist

Five remiges	
No. of remiges	Twist, deg
1-deg remiges	8.5
2-deg remiges	8.5
3-deg remiges	8.5
4-deg remiges	7.5
5-deg remiges	5.5

Table 2 Three-remiges twist

Three remiges	
No. of remiges	Twist, deg
1-deg remiges	8.5
2-deg remiges	6.5
3-deg remiges	5.5

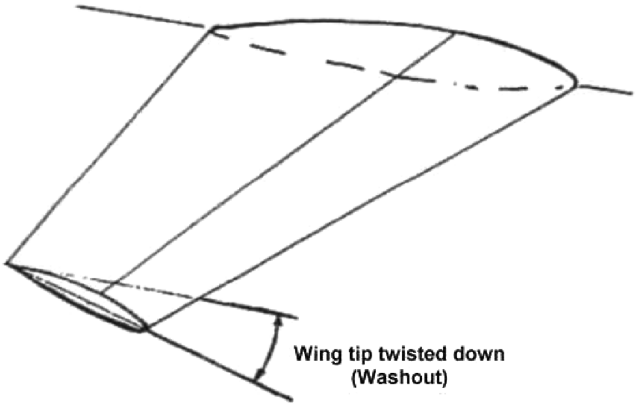

Fig. 5 Negative twist angle.

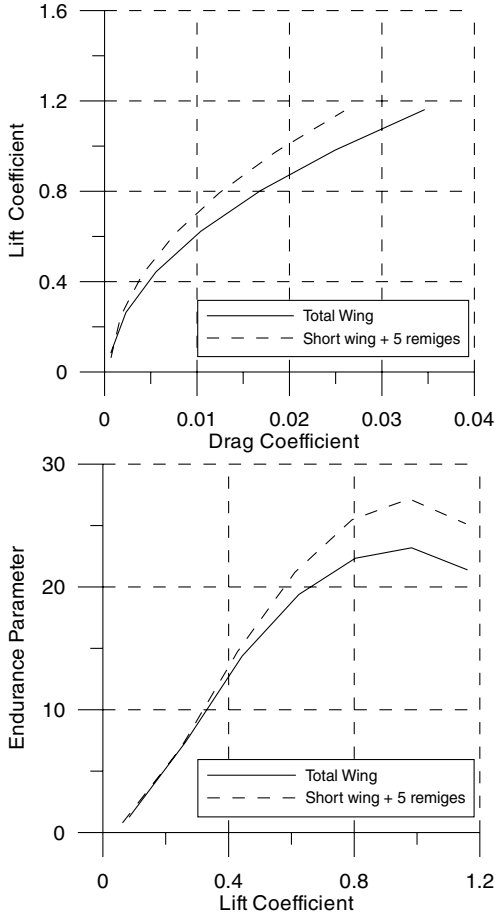

Fig. 6 Curve C_L vs C_D and endurance parameter: comparison between short wing and shortest wing + five remiges.

angles reported in these tables and in the rest of the paper must be considered negative if the winglet tip airfoil is nosed down with respect to the root winglet chord (Fig. 5). The same rule applies for pitch angles.

As Fig. 6 shows, the numerical investigation forecasts an improvement in endurance of about 17% for the configuration with five remiges. For the three-remiges configuration the predicted advantage was about 15% for endurance parameters.

III. Hang-Glider Model: Experimental Investigation

The experimental tests were carried out in the wind tunnel of the Department of Aerospace Engineering of the University of Naples Federico II. The wind tunnel is a closed circuit tunnel with closed test section. The test section has the following dimensions: width 2 m and height 1.4 m with a turbulence level of 0.1% and maximum speed of 45 m/s.

Taking into account the dimensions of the test section, an experimental semispan model of the hang-glider wing was designed and built. The model was built at the ELASIS Fiat Research Center in Pomigliano (Naples, Italy) using the rapid prototyping technique which is normally used to quickly fabricate a scale model of a part or an assembly using three-dimensional computer aided design (CAD) data. Rapid prototyping is a technology directly driven by a CAD model, rapidly manufacturing any complex shaped object.

A 4-cm standoff was interposed between the wind-tunnel wall and the model to avoid boundary layer wall interference on the model. The standoff was assembled on the wing model so that the aerodynamic loads on the standoff were not transferred to the wing model [14,15].

Aerodynamic forces and moments were measured in the tests. To measure these forces, a four-component strain gages balance (previously designed by the authors) (Fig. 7) outside the wind tunnel was used. The lift load cell has a maximum load capacity of about 2000 N and a sensitivity of 2.0 mV/V $\pm$ 10%; drag and pitch load cells both have a maximum load capacity of about 3000 N and a sensitivity of 2.0 mV/V $\pm$ 5%. The load cell is also capable of measuring the roll moment.

The model was designed and built in such a way to allow two different parts of the wing to be substituted with the set of remiges (Fig. 8). This made it possible to compare, with aspect ratio and span being kept equal, the following configurations: 1) total wing, with the short wing plus the set of remiges; and 2) short wing with the shortest wing plus the set of remiges. The geometrical characteristics of the wing semispan models are reported in the Table 3.

As described above, two different winglet sets were designed. In order to install these on the wing, a special wing tip was designed which allowed cant and pitching angles of the remige to be changed (Fig. 9). The sets of remiges and the wing tip were also built at the ELASIS Fiat Research Center of Pomigliano (NA) using the rapid prototyping technique. In the following tables (Tables 4–6) the different configurations tested and the geometrical characteristics of the remiges are summarized.

The remiges were numbered as shown in Fig. 10 from the leading edge to the trailing edge and a similar numeration was adopted for the configuration with three winglets.

In the first phase of the experimental work a preliminary investigation was carried out to optimize winglet pitch in the various winglet configurations. This investigative phase was done on both short and shortest wing configurations (Fig. 11). The results of this optimization are summarized in the Tables 7–9. The pitch angle indicated is the angle between the root chord of winglets and the main wing tip chord (positive if nose up). The deformability of winglets prompted our decision to carry out the tests using a freestream velocity of 24 m/s. At this velocity the average Reynolds number was $\sim$500, 000 on the wing and $\sim$40, 000 on the winglets.

The level of uncertainty was calculated for every point of measurement. The average of uncertainty values calculated during

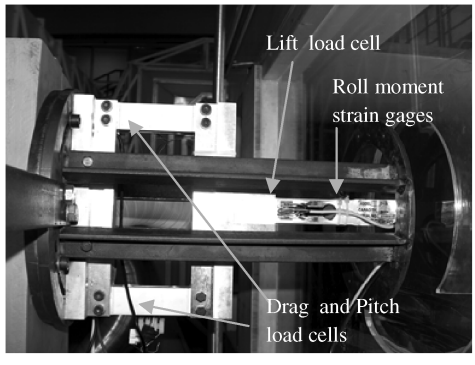

Fig. 7 Four components strain gages balance.

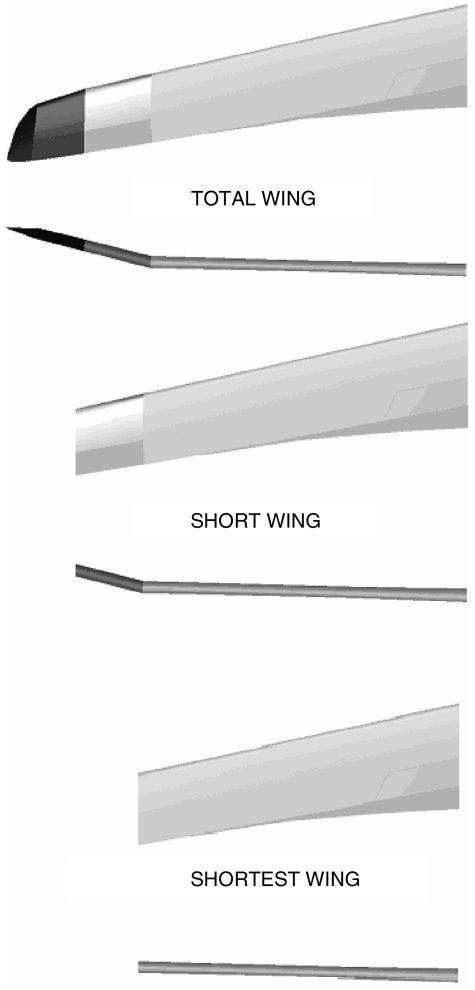

Fig. 8 Wing model settings.

the measurement phase was $\pm 0.2\%$ for C_L, and $\pm 4\%$ for C_D. In proximity of the stall condition the uncertainty of measurements was about $\pm 4\%$ for C_L, and $\pm 14\%$ for C_D; this is due to the heavy wing vibrations that occur in a stalled condition.

The junction gap between the winglets root and the wing tip was filled with a molded clay to avoid an excessive reduction of the aerodynamic performance in terms of drag due to the junction interference, and a significant influence of this fairing on the global performance was noticed.

Once the tests results had been collected they were analyzed using a reference surface for the aerodynamic loads. The reference surface was the real wing planform area, which differed depending on the configuration, and a common reference surface, which was the same for all configurations, to analyze both the aerodynamic and flying performance of the different wing arrangements. Thus, by referring the aerodynamic coefficient to the same common planform area for all configurations, we enabled the shortest wing plus the set of winglets to be compared with the total wing configuration in terms of net forces, a more useful way of comparing the flying performance of two wings with different planform areas. The same common reference surface used to normalize the aerodynamic loads and to compare flying performance is the total wing planform area 0.42 m^2. Clearly, when comparing the short wing configuration plus the set of winglets with the total wing configuration it is not necessary to make this distinction because the two configurations have essentially the same planform area.

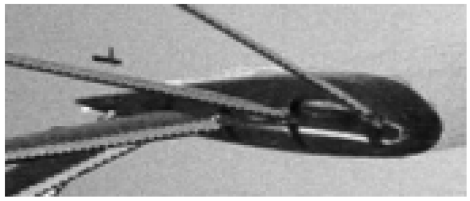

Fig. 9 Remiges configuration wing tip.

A comparison of the configuration with the same span in terms of C_L vs α showed an improvement in $C_{L\alpha}$ for the configuration with the remiges (Fig. 12). This finding is in agreement with the predicted improvement of the remiges configuration in terms of induced drag and consequently of wing downwash and was also observed in [8].

During the optimization phase it was observed that the five-remiges configuration seemed to have a better behavior than the three-remiges configuration. These early observations were confirmed by the first experimental tests on the optimized configurations (for both five- and three-winglets cases). After these results, for the following tests, more attention was paid to the test with five-remiges configurations, but, however, the test outcomes regarding the three-remiges case are reported in the result tables.

As shown in Figs. 13 and 14 the configurations with winglets yielded an improvement in terms of C_D starting from values of $C_L \sim 0.35$ and $C_L \sim 0.28$, respectively, for the comparison between the short wing plus five remiges with the total wing and for the comparison between the shortest wing plus five remiges with the short wing. Obviously there is worse performance of the wings with remiges for low αs probably due to a higher parasite drag of the wing with the remiges with respect to the configurations without the remiges, but it is important to remark here that 1) in this work we have not paid particular attention to improve the parasite drag of the remiges configuration (for example, adopting a well-designed junction between the remiges root and the wing tip); and 2) flying with the shortest wing plus the remiges, the flying αs will be higher with respect to the total wing due to the different planform area.

Figure 15 shows the comparison between the endurance parameter of the total wing and the endurance parameter of the shortest wing plus five remiges. As stated above, this comparison was carried out with reference to the aerodynamic coefficient of both configurations to the total wing planform area. From Fig. 15 it is evident that it is possible to fly with the shortest wing plus five remiges without any loss in performance and with clear gain in terms of weight, bending moment, and maneuverability.

Tables 10–12 summarize the results for all the tested configurations in terms of Oswald factor and percentage gain.

Table 4 Configurations tested

Configurations	Semisurface, m^2	Semispan, m	AR
Short wing + five remiges	0.40	1.65	13.6
Shortest wing + five remiges	0.34	1.39	11.20
Short wing + three remiges	0.39	1.65	13.7
Shortest wing + three remiges	0.34	1.39	11.22

Table 3 Geometrical characteristics of the wing semispan models

	Semisurface, m^2	Semispan, m	AR	Root chord, m	Tip chord, m	Twist, deg
Total wing	0.42	1.65	12.8	0.36		5 deg
Short wing	0.35	1.37	10.65	0.36	0.24	4 deg
Shortest wing	0.29	1.12	8.5	0.36	0.22	3 deg

Table 5 Five-remiges set

No. of remige	Surface, m^2	Span, m	Twist, deg	Taper ratio	Root chord, m
1-deg remige	0.01	0.25	8.5	1	0.04
2-deg remige	0.01	0.25	8.5	1	0.04
3-deg remige	0.01	0.25	8.5	1	0.04
4-deg remige	0.01	0.25	7.5	1	0.04
5-deg remige	0.01	0.25	5.5	1	0.04

Table 6 Three-remiges set

No. of remige	Surface, m^2	Span, m	Twist, deg	Taper ratio	Root chord, m
1-deg remige	0.015	0.25	8.5	0.53	0.07
2-deg remige	0.015	0.25	6.5	0.53	0.07
3-deg remige	0.015	0.25	5.5	0.53	0.07

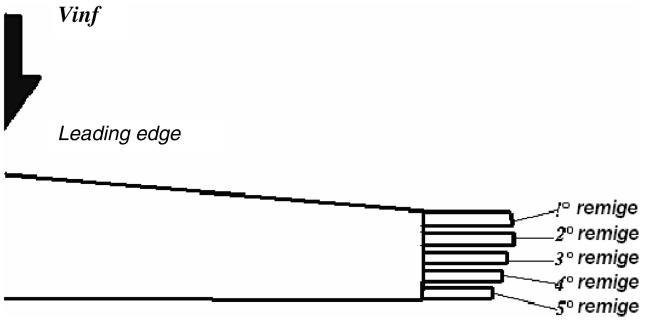

Fig. 10 Remiges numbering.

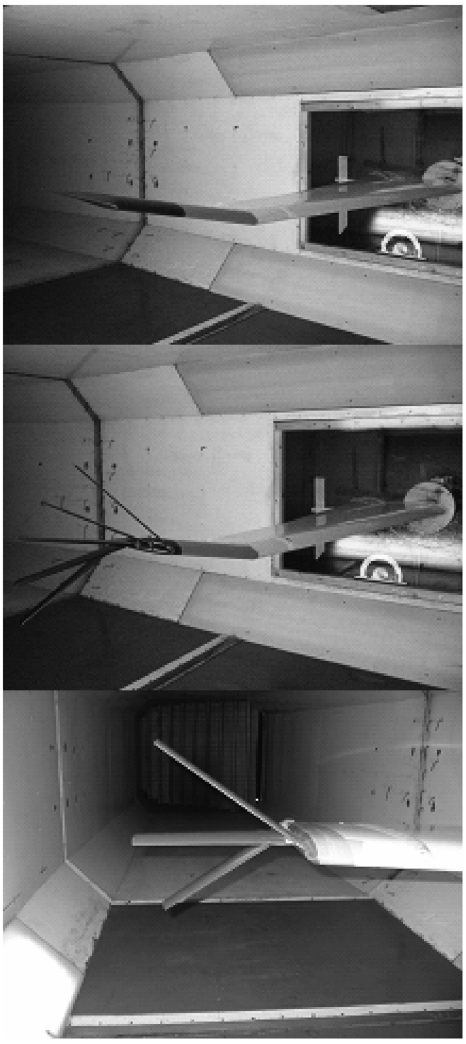

Fig. 11 Some of the tested wing configurations.

Table 7 Optimization results

Short wing + five remiges		
No. of remige	Cant angle	Pitch
1-deg remige	43.5 deg	−10 deg
2-deg remige	26.5 deg	−4 deg
3-deg remige	12 deg	−14 deg
4-deg remige	−9 deg	−8 deg
5-deg remige	−30 deg	−6 deg

Table 8 Optimization results

Shortest wing + five remiges		
No. of remige	Cant angle	Pitch
1-deg remige	33 deg	−17 deg
2-deg remige	16 deg	−10 deg
3-deg remige	−1 deg	−10 deg
4-deg remige	−17 deg	−6 deg
5-deg remige	−39.5 deg	−4 deg

Table 9 Optimization results

Short and shortest wing + 3 remiges		
No. of remige	Cant angle	Pitch
1-deg remige	43.5 deg	−6.5 deg
2-deg remige	26.5 deg	−4.5 deg
3-deg remige	−12 deg	−4.5 deg

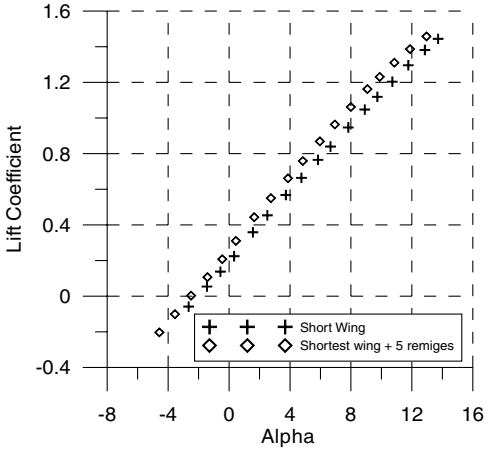

Fig. 12 Curve C_L vs α: comparison between total wing and short wing + five remiges. Planform surface of each wing has been used as a reference area in the coefficients.

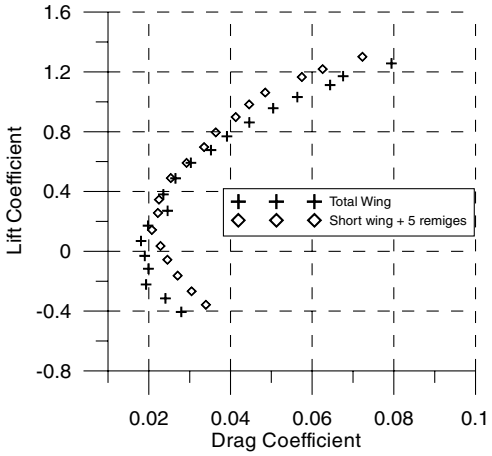

Fig. 13 Curve C_L vs C_D: comparison between total wing and short wing + five remiges. Planform surface of each wing has been used as a reference area in the coefficients.

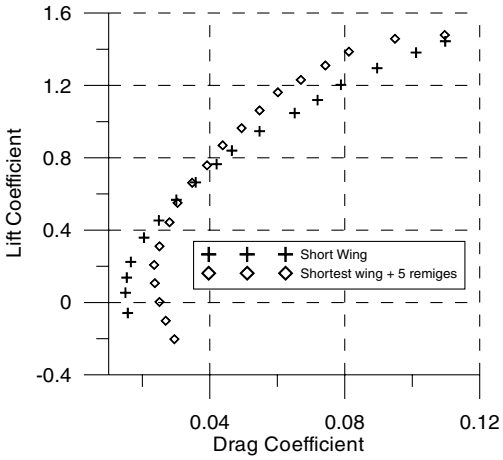

Fig. 14 Curve C_L vs C_D: comparison between short wing and shortest wing + five remiges. Planform surface of each wing has been used as a reference area in the coefficients.

The Oswald factor in Table 10 is computed by referring all the configurations to their own planform area, while in Tables 11 and 12 all the coefficients were computed using the total wing planform area as a reference surface.

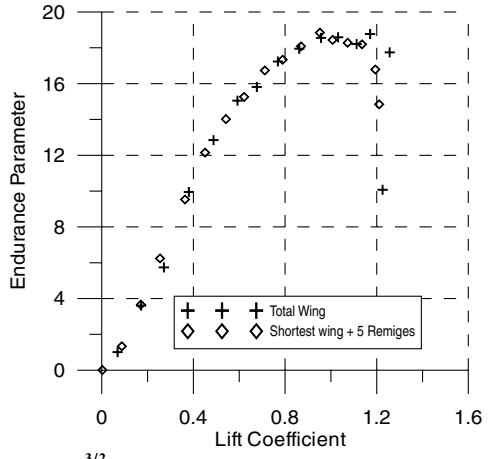

Fig. 15 Curve $C_L^{3/2}/C_D$ vs C_L: comparison between total wing and short wing + five remiges. Coefficients referred to the same wing planform area.

Table 10 Oswald factor (planform surface of each wing has been used as a reference area in the coefficients)

Configuration	*AR*	*e*
Total wing	12.80	0.68
Short wing	10.65	0.78
Shortest wing	8.50	0.84
Short wing + five remiges	13.60	0.87
Shortest wing + five remiges	11.20	0.94
Shortest wing + three remiges	11.20	0.90

Table 11 Comparison with total wing (coefficient referred to the total wing planform area)

	Fixed C_L	% advantage in comparison with total wing	
Configuration	C_L	C_D	$C_L^{3/2}/C_D$
Short wing + five remiges	$\sim$1	-17%	$+18\%$

Table 12 Comparison with short wing (coefficient referred to the total wing planform area)

	Fixed C_L	% advantage in comparison with short wing	
Configuration	C_L	C_D	$C_L^{3/2}/C_D$
Shortest wing + five remiges	$\sim$1	-13%	$+15\%$
Shortest wing + three remiges	$\sim$0.8	-12%	$+11\%$

IV. Elliptical Wing Model: Experimental Investigation

To verify the effectiveness of remiges in comparison with a well-defined span load, a semimodel of an elliptical wing was built. The model was built keeping the leading edge straight, and it was possible to replace a part of the wing with the set of remiges as done on the previously tested wing (Fig. 16).

The wing airfoil used is the NFL 1015. This airfoil shows maximum endurance at low C_L and a $C_{L\alpha} = 0.1/\deg$. The geometrical characteristics of the elliptical wing semispan model are reported in Table 13. This time, the wing was also equipped with 122 pressure holes in order to check the span load distribution.

The pressure holes were distributed over 17 wing sections. It was not possible to distribute a sufficient number of pressure holes over all of the sections as this would have required more tubes than was physically possible to fit inside the wing. For this reason it was chosen to distribute 36 pressure holes on three wing sections placed at 25, 50, and 80% of the wing, and the others on the wing upper surface on the remaining sections.

The pressures were measured using two different pressure transducer systems each equipped with 64 ports and made by

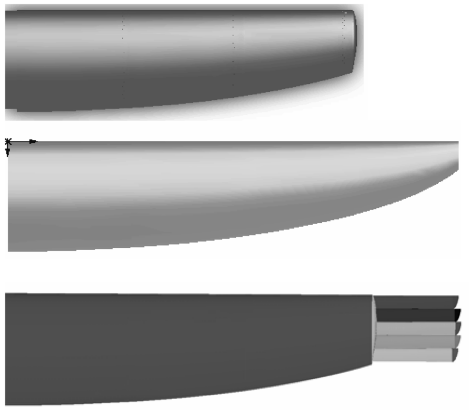

Fig. 16 Elliptical wing model: total, short wing and short wing + five remiges.

Table 13 Geometrical characteristics

	b, m	S, m^2	Cr, m	Ct, m	AR
Total wing	1.51	0.4522	0.37	0.097	10.08
Short wing	1.2	0.3965	0.37	0.233	7.26

Table 14 Optimization results

Short wing + five remiges		
No. of remige	Pitch	Cant angle
1-deg remiges	−4.2 deg	13.7 deg
2-deg remiges	−2.8 deg	3.04 deg
3-deg remiges	−5.6 deg	−1.63 deg
4-deg remiges	−4.6 deg	−15.9 deg
5-deg remiges	−2.6 deg	−23.9 deg

Table 15 Optimization results

Short wing + three remiges		
No. of remige	Pitch	Cant angle
1-deg remiges	−5.4 deg	43 deg
2-deg remiges	−4.9 deg	10 deg
3-deg remiges	−1.6 deg	−20.6 deg

Scanivalve Corporation with a full-scale (FS) range of ∼2550 Pa and an accuracy of about 3.8 Pa (0.15% of full-scale range).

The same sets of remiges used for the previous hang-glider wing tests were applied to the short wing model. As in the hang-glider tests, a preliminary phase of winglet pitch optimization was carried out. The parameter optimized was the $C_L^{3/2}/C_D$, and the optimization was performed at an angle of attack of 6 deg, which was the angle of maximum $C_L^{3/2}/C_D$ for the total wing. The results of this investigation are reported in Tables 14 and 15.

For the same reasons described in the previous section, the tests were carried out using a freestream velocity of 25 m/s corresponding to an average Reynolds number of ∼500, 000 on the wing (referred to as the mean aerodynamic chord) and ∼40, 000 on the winglets.

A. Elliptical Wing: Discussion of Results

A first series of tests was carried out on the total wing without winglets to check the elliptical span load. The curves C_L vs α and C_L vs C_D are reported in Figs. 17 and 18. The shape of the curve C_L vs α reflects the shape of the airfoil curve NFL 1015 showing a change in the curve slope before the stall angle. As expected, the wing α_{oL} is

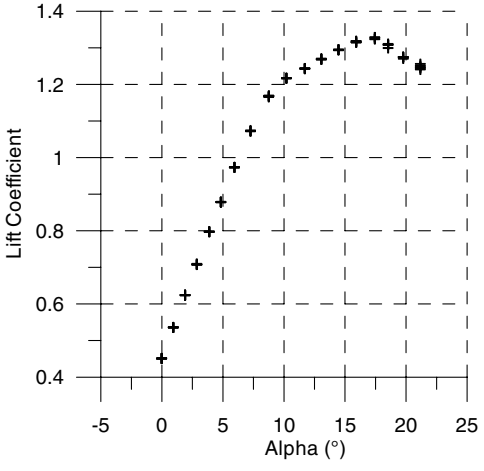

Fig. 17 Total wing: C_L vs α curve.

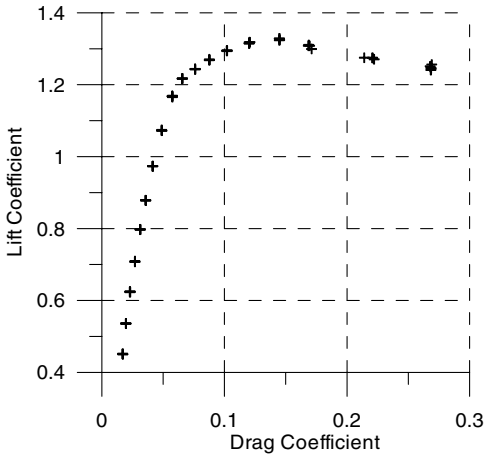

Fig. 18 Total wing: C_L vs C_D curve.

equal to the airfoil $\alpha_{ol} \sim -6$ deg. Computing the slope of C_L vs α using the experimental data curve in the linear range gives $C_{L\alpha} = 0.087/\text{deg}$. From the elliptical wing theory the result is

$$C_{L\alpha} = \frac{C_{l\alpha}}{1 + C_{l\alpha}/(\pi \cdot AR)} = 0.085/\text{deg}$$

The comparison between the theoretical and the experimental $C_{L\alpha}$ is therefore fairly satisfactory.

The Oswald factor computed from the experimental data comes out as $e = 0.94$. This was considered reasonable supposing that the difference between the theoretical ($e = 1$) and the experimental results could be due to the Oswald factor being calculated by considering the viscous drag constant with α while in reality it is not. Using the pressure test results it is possible to compute the local span load cC_1 in the section at 25, 50, and 80% of the span. The comparison between the experimental and the theoretical span load (elliptical wing theory) is once again satisfactory (see Fig. 19).

Once the total wing had been fully characterized, the experimental tests on the configurations with the remiges were carried out. In this case, the configuration with the winglet does not seem to be advantageous in comparison with the total wing as in the case of the hang glider. As found for the hang-glider wing, the configuration with three winglets did not show any improvement over the total wing, whereas that with five remiges showed an improvement for values of $C_L > 0.65$ (Figs. 20 and 21). Tables 16 and 17 summarize the main results obtained from the comparison between the different configurations.

B. Elliptical Wing: Wake Survey

A wake survey was performed to investigate the wake vortex structure downstream of the wing. This investigation was carried out using a five-hole probe. The probe was positioned about two and one-half chords downstream of the wing trailing edge and placed on a two-axes moving system controlled by a dedicated PC (Fig. 22).

For every point of measurement the probe supplied the three velocity components (u, v, w), while the spatial positions (x, y, z)

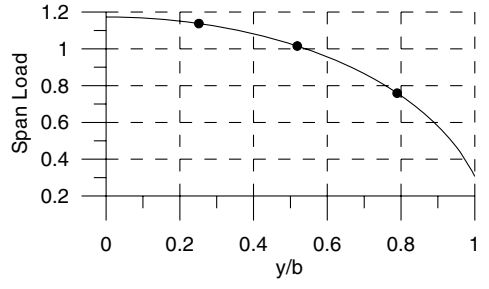

Fig. 19 Comparison between theoretical and experimental span load: $\alpha = 3$ deg.

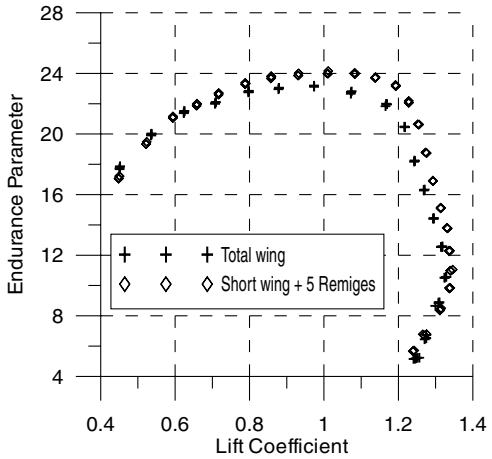

Fig. 20 Curve $C_L^{3/2}/C_d$ vs C_L: comparison between elliptical wing configuration and five-remiges configuration.

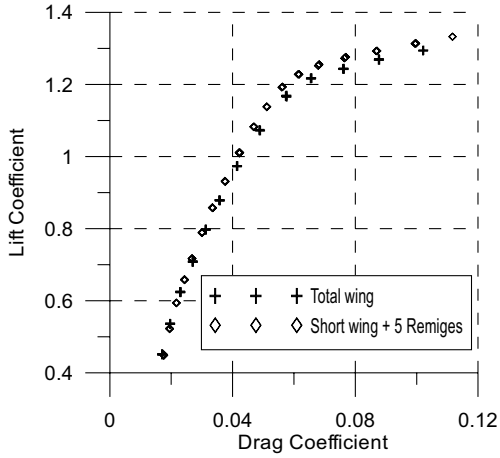

Fig. 21 Curve C_L vs C_D: comparison between elliptical wing configuration and five-remiges configuration.

were supplied by the movement control system. In this way it was possible to scan the velocity field in a plane downstream of the wing orthogonal to freestream velocity.

The investigation was carried out for both the elliptical wing configuration and for the five-remiges wing configuration, both at an angle of attack of 6 deg. The points of measurement were distributed on a structured grid on the scanning plane. The first measurement was carried out on a 1200 point grid. The measurement time for this grid took about one and one-half hours. The grid measurement external sizes were 1200 mm in width and 600 mm in height with a spacing of 30 mm. The use of these grid dimensions to scan the wake plane made it possible to identify the vortex structures downstream of the elliptical wing configuration and downstream of the five-remiges wing configuration (Figs. 23 and 24).

Once the position of the vortices had been identified, a more accurate wake scan was carried out on the five-remiges wing configuration in the zones where vortices were present. The grid dimensions used in this case were 600 mm in width and 600 mm in height with a grid spacing of 10 mm (3600 points) (Fig. 25).

As Fig. 26 shows, the five-remiges configuration shows the wing tip vortex to be split into five vortices, which, as expected, have a lower intensity of vorticity compared with the elliptical wing vortex. It should be noted that the vorticity value indicated in Fig. 26 is the mean value of vorticity for each grid cell.

To obtain a qualitative estimate of the induced drag for the two different configurations, the Maskell formula [16] was applied to the scanned planes.

Table 16 Oswald factor

Configurations	*AR*	*e*
Total wing	10.04	0.94
Short wing + five remiges	9.96	1.04
Short wing + three remiges	10.03	0.83

Table 17 Comparison with elliptical wing

	Fixed C_L	% advantage		
	C_L	C_D	C_L/C_D	$C_L^{3/2}/C_D$
Short wing + five remiges	1.2	−8%	+10%	+9%

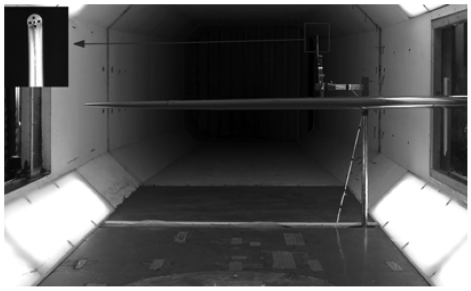

Fig. 22 Elliptical wing: wake survey.

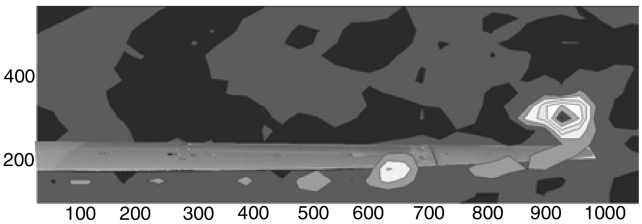

Fig. 23 Elliptical wing: vorticity.

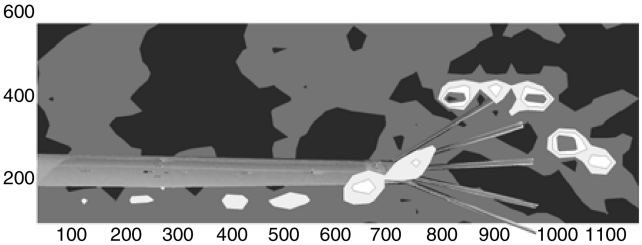

Fig. 24 Five-remiges configuration: vorticity (1200 × 600 mm).

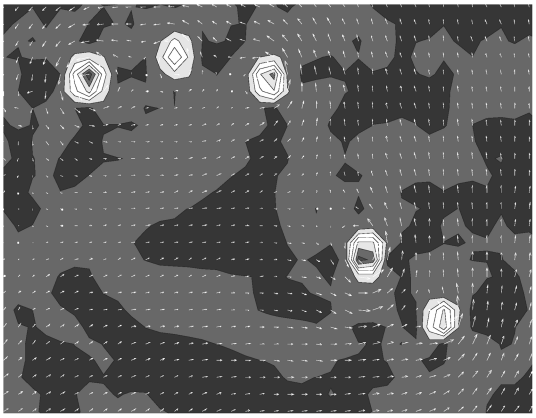

Fig. 25 Five-remiges configuration: vorticity and velocity vectors (600 × 600 mm).

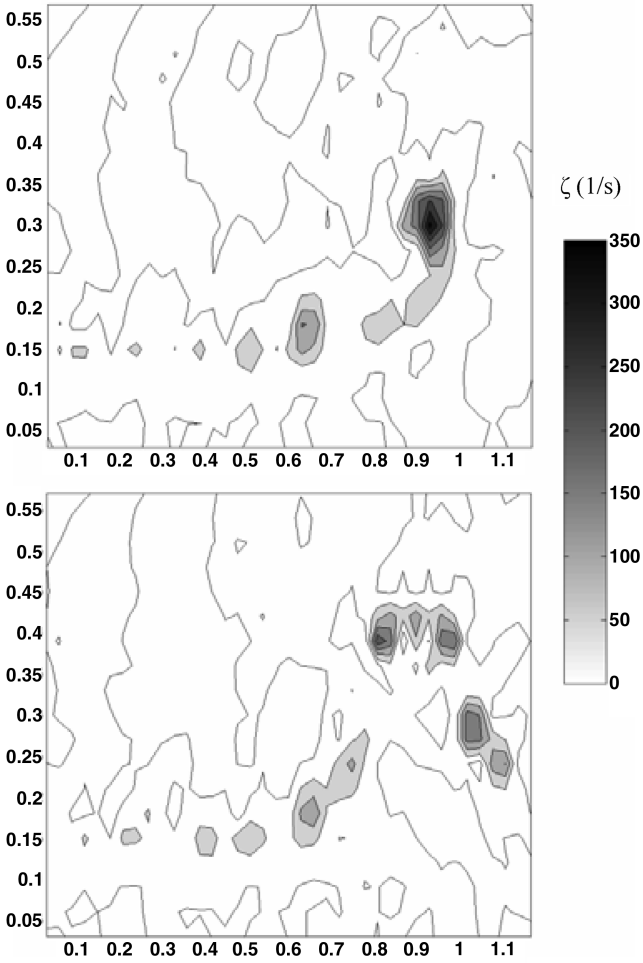

Fig. 26 Comparison between elliptical wing and five-remiges vorticity intensity.

$$D_i = \frac{1}{2}\rho \iint_W \psi \cdot \zeta \, \mathrm{d}y \, \mathrm{d}z$$

where ψ comes from the solution of the Poisson equation: $\nabla^2\psi = -\xi$.

A comparison of the results from the Maskell analysis, reported in Table 18, shows an induced drag reduction of 13% for the five-remiges configuration.

V. Conclusions

An experimental investigation on a hang-glider wing model equipped with opportunely designed multiple winglets was carried out. The design used for the winglets is reminiscent of the feathers at the tip of a bird's wing: the remiges. Two different configurations with three and five remiges were designed. In the design phase, the length, the twist, and the cant angle of the remiges were ascertained using a vortices lattice computational code. An experimental comparison with an elliptical wing was also carried out to verify the effectiveness of these devices.

In the case of the hang glider the results obtained seem highly promising. The maximum gain achieved in terms of endurance was about 18% for the five-remiges configuration. This advantage was not obtained in comparison with the elliptical wing. In the latter case the maximum advantage achieved in terms of endurance was about 9%; this result was also obtained for the five-remiges configuration.

Table 18 Comparison of the results from the Maskell analysis

Configuration	C_{Di}
Elliptical wing	0.0168
Five remiges	0.0146

Wake surveys of the elliptical wing with no winglets and with five remiges were also performed using a five-hole probe. From the five-remiges configuration wake survey it was possible to distinguish five separate vertically spread vortices. Evaluation of induced drag with the Maskell formula confirmed the gain of five-remiges configuration with respect to the clean elliptical wing.

Acknowledgments

This work has been partially sponsored by ELASIS Fiat Research Center. We thank N. Di Giusto, A. D'Arrigo, G. Monacelli, and G. Tortora for their collaboration.

References

[1] Whitcomb, R., "A Design Approach and Selected Wind-Tunnel Results at High Subsonic Speeds for Wing-Tip Mounted Winglets," NASA TN D-8260, July 1976.

[2] Whitcomb, R., "Method for Reducing Aerodynamic Drag," NASA CP 2211, Dryden Symposyum, Sept. 1981.

[3] Mortara, K. W., and Maughmer, M. D., "A Method for the Prediction of Induced Drag for Planar and Nonplanar Wings," AIAA Paper 1993 3420-CP.

[4] Spillman, J. J., "The Use of Wing Tip Sails to Reduce Vortex Drag," *Aeronautical Journal*, Vol. 82, No. 813, Sept. 1978, pp. 387–395.

[5] Spillman, J. J., Ratcliffe, H. Y., and McVitie, A., "Flight Experiments to Evaluate the Effect of Wing-Tip Sails on Fuel Consumption and Handling Characteristics," *Aeronautical Journal*, Vol. 83, July 1979, pp. 279–281.

[6] Zimmer, H., "The Aerodynamic Optimization of Wings at Subsonic Speeds and the Influence of Wingtip Design," NASA TM-88534, 1987.

[7] La Roche, U., and La Roche, H. L., "Induced Drag Using Multiple Winglets, Looking Beyond the Prandtl-Munk Model," AIAA Paper 2004-2120, 2004.

[8] Smith, M. J., Komerath, N., Ames, R., Wong, O., and Pearson, J., "Performance Analysis of a Wing with Multiple Winglets," AIAA Paper 2001-2407, 2001.

[9] Shelton, A., Tomar, A., Prasad, J. V. R., Smith, M., and Komerath, N., "Active Multiple Winglets for Improved Unmanned-Aerial-Vehicle Performance," *Journal of Aircraft*, Vol. 43, No. 1, 2006, pp. 110–116.

[10] Catalano, F. M., and Ceron-Munoz, H. D., "Experimental Analysis of Aerodynamics Characteristics of Adaptive Multi-Winglets," AIAA Paper 2005-1231, 2005.

[11] Smith, S. C., "A Computational and Experimental Study of Nonlinear Aspects of Induced Drag," NASA, TP 3598, 1996.

[12] Kroo, I., "Drag Due to Lift: Concepts for Prediction and Reduction," *Annual Review of Fluid Mechanics*, Vol. 33, Jan. 2001, pp. 587–617. doi:10.1146/annurev.fluid.33.1.587

[13] Katz, and Plotkin, *Low Speed Aerodynamics, From Wing Theory To Panel Methods*, McGraw–Hill, New York, 1991.

[14] Gatlin, G. M., and Mcghee, R. J., "Study of Semi-Span Model Testing," AIAA Paper 96-2386, 1996.

[15] Gatlin, G. M., Parker, P. A., and Owens, L. R., Jr., "Development of a Semi-Span Test Capability at the National Transonic Facility," AIAA Paper 2001-0759, 2001.

[16] Coiro, D. P., Nicolosi, F., De Marco, A., Scherillo, F., and Maisto, U., "Induced Drag of an America's Cup Yacht's Fin-Bulb-Winglet: Numerical and Experimental Investigation," *7th High Speed Marine Vehicles Conference*, Conference Proceedings, Naples, Italy, 21–23 Sept. 2005.